Chalcogenide Letters Vol. 22, No. 9, September 2025, p. 847 - 854

Cu_2MgSnS_4 thin films: a promising absorber material for next-generation solar cells

Y. B. K. Kumar [a,*], S. G. Prasad [b], A. S. S. Smitha [c], S. M. Naidu [d], G. S. Babu [c], P. U. Bhaskar [e], U. Chalapathi [f,*]

[a] *Solar Energy Laboratory, Mohan Babu University (Erstwhile Sree Vidyanikethan Engineering College), Tirupati-517102, India*

[b] *Department of Physics, N.T.R. Government Degree College, Vayalpad-517299, India*

[c] *Department of Physics, Government Degree College, Puttur-517583, India*

[d] *Department of Physics, Vel Tech Rangarajan Dr. Sagunthala R&D Institute of Science and Technology (Deemed to Be University), Avadi, Chennai-600062, India*

[e] *Mundra Solar Technology LTD (Adani Solar), Mundra, Gujarat-370435, India*

[f] *Department of Electronic Engineering, Yeungnam University, 280 Daehak-Ro, Gyeongsan, Gyeongbuk, 38541, South Korea*

Cu_2MgSnS_4 thin films have emerged as potential candidates for use in photovoltaic applications owing to their direct band gap properties. These quaternary compounds are fabricated through the spray pyrolysis method at 175 °C, utilizing two different carrier gases, such as air and nitrogen. After pyrolysis, deposited films are annealed at 450 °C for 1 hour. Structural analysis confirms the films exhibit a tetragonal kesterite structure. Using nitrogen as the carrier gas results in a larger crystallite size, accompanied by a reduction in both the dislocation density and microstrain. Raman spectroscopy further validates phase purity. Surface morphology analysis indicates a more compact grain structure in films deposited under nitrogen. Optical measurements reveal a strong absorption coefficient and a direct band gap of approximately 1.55 eV for nitrogen-grown samples. Cu_2MgSnS_4-based solar cells demonstrate promising optoelectronic characteristics.

(Received June 11, 2025; Accepted September 25, 2025)

Keywords: Cu_2MgSnS_4, Spray method, Carrier gas, Structural studies, Optical properties

1. Introduction

Electricity is essential for industries, transport, medicine, communication networks, etc. In general, it is produced from fossil fuels and nuclear energy. However, the combustion of fossil fuels releases CO_2, contributing to global warming and environmental degradation [1]. As a solution, there is a growing reliance on renewable energy options like solar, wind, and hydro power. Among them, solar energy stands out due to its ability to convert sunlight directly into electricity using solar cells. The silicon-based solar cells, first introduced in the 1950s, offer good efficiency, but they are costly and perform less effectively under low-light conditions. Thin film solar cells were developed to overcome the above constraints [2].

Cadmium telluride (CdTe) and Copper indium gallium selenide (CIGS) have been established as reliable and effective technologies for solar energy conversion. CdTe has environmental issues owing to the toxicity of cadmium. CIGS cells have high efficiency but are complicated and expensive to manufacture [3]. Copper zinc tin sulfide solar cells consist of cheap and non-toxic chemicals, but they are relatively less efficient when compared to CdTe and CIGS. Copper magnesium tin sulfide (Cu_2MgSnS_4) is a new material that has the advantage of earth-abundant, non-toxic components with enhanced stability, in terms of inexpensive and green solar cell absorber material for new-generation solar cells. Cu_2MgSnS_4 (CMTS) possesses a direct bandgap of about 1.6 eV, making it well-suited for photovoltaic applications [4]. It exhibits a high

* Corresponding author: chalam.uppala@gmail.com
https://doi.org/10.15251/CL.2025.229.847

absorption coefficient in the visible spectrum, permitting efficient light capture in thin films. Substitution of Zn with Mg in Cu_2ZnSnS_4 decreases Cu-II anti-site defects, a prevalent source of cation disorder, and also enhances the crystal quality, charge carrier transport, and minimizes recombination losses [5]. CMTS crystallizes in a tetragonal phase with stannite/kesterite structure, which is compatible with conventional thin film deposition techniques.

To date, the work done on Cu_2MgSnS_4 thin films is meager. A few researchers effectively deposited Cu_2MgSnS_4 thin films using the spray pyrolysis method. Souli et al. reported that the best grain size was achieved at 175 °C, and annealing at 450 °C minimizes the secondary phases in the film. The bandgap of the deposited films was 1.35 eV, and the films exhibit an absorption coefficient of about 10^5 cm^{-1} [6]. Sarra et al. synthesized these films at 360 °C and reported the structure as stannite, and the energy gap as 1.64 eV [7]. Rafal et al. demonstrated that films deposited at 400 °C with 0.20 M thiourea exhibited the best crystallinity, and all samples had a p-type nature [4]. Hammoud et al. optimized Mg content at 210 °C and obtained uniform films with a narrowed bandgap of 1.50 eV [8]. In another study, Hammoud et al. found that optimal sulfur concentration (40 m mol/L) increases the photocatalytic activity [9]. Aravind et al. enhanced film quality through annealing up to 375 °C, broadening the bandgap from 2.5 eV to 2.02 eV. They prepared CMTS thin-film solar cells, which exhibited good electrical performance [10].

Gang et al. deposited Cu_2MgSnS_4 thin films using the sol-gel technique followed by sulfurization. They reported the enhanced crystallinity and a narrower bandgap at higher annealing temperatures. Optimal sulfurization at 530 °C provided a solar cell efficiency of 0.78% [11]. Zitti et al. synthesized through sol-gel dip-coating without sulfurization and achieved a stannite structure with (112) orientation. Annealing at 475 °C improved optical and electrical characteristics, yielding a 1.5 eV bandgap and 1.17 Ωcm^{-1} conductivity [12]. Akash et al. prepared these films using spin coating and investigated the influence of drying temperatures. Uniformity and crystallinity increased to 300 °C, and the bandgap reduced from 1.999 to 1.775 eV. The Photocurrent density increased by 472% at 300 °C, showing promising photoelectrochemical devices [13]. Yixin et al. deposited these films by an ultrasonic co-spray pyrolysis technique onto lime glass substrates at 350 °C to yield uniform films with excellent surface quality and phase purity [14]. Ming et al. were able to synthesize highly crystalline CMTS nanoparticles using a hot-injection approach, allowing for tunable particle size and purity [15]. Ahsan et al. employed a co-precipitation route for synthesizing CMTS nanoparticles [16]. Guan et al. precipitated CMTS nanoparticles from a solvothermal process, which supported fine control over particle size and crystallinity [17].

In the current study, Cu_2MgSnS_4 films were deposited using the spray pyrolysis method by utilizing two different carrier gases. The impact of the carrier gas on the spray-pyrolyzed films was extensively examined and discussed. Spray pyrolysis is considered an economical and flexible approach for thin film deposition. This method is effective for producing uniform thin films suitable for a range of applications such as solar cells, sensors, and protective coatings [18].

2. Experimental

Cu_2MgSnS_4 films were synthesized using the spray pyrolysis method, starting from a precursor solution comprising cupric chloride (10 mM), magnesium chloride (5 mM), stannic chloride (4 mM), and thiourea (30 mM). An excess of thiourea was added to offset sulfur volatilization during thermal decomposition. Methanol was used as the solvent in this study to reduce the generation of oxide phases during film deposition. The precursor solution was sprayed using a stainless-steel spray nozzle (Model: ¼ JAU, Spraying Systems Co., USA) and deposited on preheated glass substrates at an optimized temperature of 175 °C [5]. The impact of carrier gas type on film growth was investigated by using pure air and nitrogen separately. Substrate temperature was controlled and measured with a digital temperature controller. The detailed experimental setup was described in earlier publications [1,3]. After deposition, the thin films were annealed at the optimized temperature and time to improve their structural and compositional quality. Annealing was done in a sulfur ambient with a dual-zone tubular vacuum furnace. The CMTS films were kept inside the first heating zone, and high-purity sulfur pellets (Sigma-Aldrich) were placed inside the second zone. The first zone was ramped up at 10 °C/min until 450 °C and

was maintained for 1 hour [5]. At the same time, the second zone with the sulfur source was kept around 125 °C to maintain enough sulfur vapor pressure. The sulfur pellets were placed in a molybdenum boat, while the CMTS films were loaded onto a graphite boat. Following annealing, the furnace temperature was slowly decreased at a rate of 10 °C/min until it reached 120 °C. After that, the setup was left to cool naturally to room temperature. The detailed experimental configuration was discussed in our earlier publications [19,20].

Structural analysis was carried out by X-ray diffraction (XRD) in Bragg-Brentano geometry with Cu-Kα radiation (λ = 0.15406 nm) on a Bruker diffractometer. Structural analysis was also performed with Raman spectroscopy. Optical transmittance and reflectance spectra were measured between 300 and 1500 nm with a Jasco UV–Vis–NIR spectrophotometer. Microstructural properties were analyzed using scanning electron microscopy (SEM), and elemental analysis was evaluated using energy dispersive spectroscopy.

3. Results and discussion

Table 1 presents the elemental content of Cu_2MgSnS_4 thin films prepared using 2 carrier gases. A decrease in copper content was observed in the films deposited with nitrogen, which is advantageous for the inhibition of the development of undesirable secondary phases [21,22]. The atomic percentage for magnesium was slightly higher in the nitrogen-based deposition, reflecting enhanced incorporation of this element under inert conditions. Most significantly, sulfur content increased when nitrogen was used in pyrolysis. This enhancement is most probably due to the inert character of nitrogen, which suppresses oxidation during deposition and facilitates better sulfur retention in the film matrix [23].

Table 1. Cu_2MgSnS_4 film elemental composition.

Carreri gas	Elemental composition (at%)				$\frac{Cu}{(Mg+Sn)}$	$\frac{Mg}{Sn}$	$\frac{S}{metal}$
	Cu	Mg	Sn	S			
Air	25.68	18.83	12.88	42.61	0.810	1.462	0.742
Nitrogen	25.12	18.71	12.66	43.51	0.801	1.478	0.771

Fig. 1 shows the XRD spectra of Cu_2MgSnS_4 thin films deposited with two different carrier gases. For both sets of samples, the films demonstrate a preferred orientation along the (112) plane, with additional peaks corresponding to the (220) and (312) planes, conforming to the tetragonal phase of CMTS [7, 24]. However, films deposited using nitrogen demonstrate greater peak intensities, indicating better crystallinity. This was also identified by ratios of intensities of (112)/(220) planes and intensities of (112)/(312) planes, reflecting enhanced (112) texture and structural ordering when nitrogen was used [25]. The improvement in crystallinity may result from the low ratio of nitrogen gas weight to volume of aqueous solution, which produces fine aerosol droplets and can enhance the quality of film formation during the spray deposition process [25].

The following mathematical formulas were used for calculating the various structural parameters from the XRD spectra of CMTS films [7, 13].

$$\text{Crystallite size}(D) = \frac{0.94\,\lambda}{\beta\cos\theta} \tag{1}$$

$$\text{Dislocation density}(\delta) = \frac{1}{D^2} \tag{2}$$

$$\text{Microstrain}(\varepsilon) = \frac{\beta}{4\tan\theta} \tag{3}$$

$$\frac{1}{d} = \sqrt{\frac{h^2+k^2}{a^2} + \frac{l^2}{c^2}} \quad (4)$$

$$\text{Unit cell volume}(V) = a^2c \quad (5)$$

Here λ is the X-ray wavelength employed for XDR measurement, β is the FWHM, θ is Bragg's angle, d is the interplanar spacing, and a & c are the lattice constants. The various structural parameters are listed in Table 2; these coincide with reported values [7].

Table 2. Mathematical analysis of XRD spectra.

Carrier gas	D (nm)	δ (nm^{-2})	ε	a (nm)	c (nm)	V (nm^{-3})	Disorder parameter $^{c}/_{2a}$
Air	6.56	0.023	0.038	0.536	1.113	0.320	1.038
Nitrogen	7.73	0.016	0.022	0.539	1.082	0.314	1.003

The disorder parameters of the deposited films for both films were observed to be near unity, which is a sign of the kesterite structure. Films constructed with nitrogen as the carrier gas exhibited a $^{c}/_{2a}$ ratio trending towards 1, which is a sign of a decrease in structural defects [26]. A significant reduction in both dislocation density and microstrain was noted when nitrogen was utilized, indicating better structural quality. Increased crystallinity in the films generally corresponds to a reduced dislocation density [27,28].

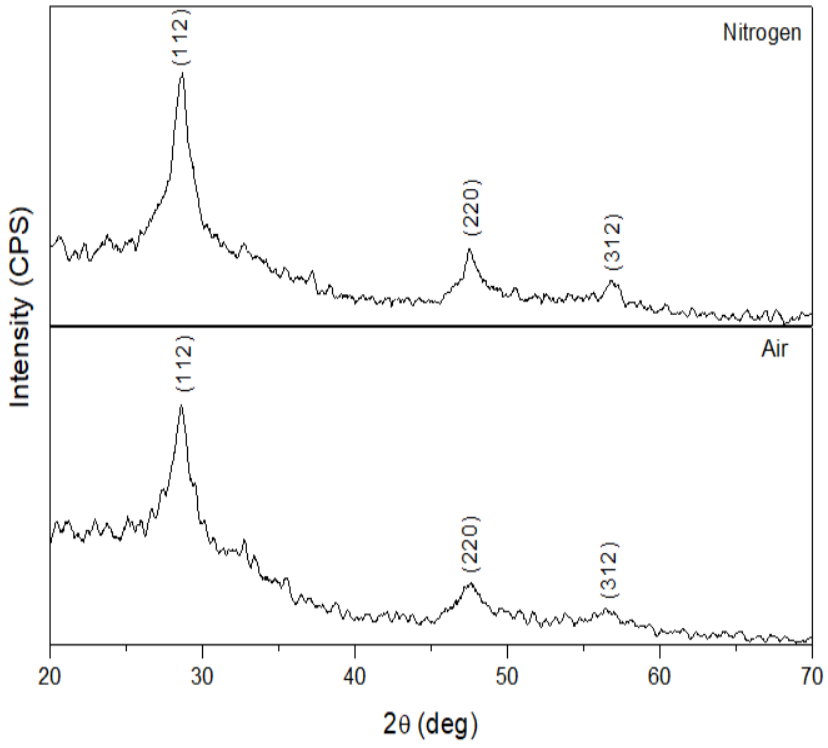

Fig. 1. XRD spectra of Cu_2MgSnS_4 films deposited with air and nitrogen carrier gases.

Fig. 2 shows the Raman spectrum of Cu_2MgSnS_4 films prepared by using nitrogen. A dominant Raman mode was observed at 333 cm^{-1}, which is a sign of the Cu_2MgSnS_4 phase [7,15]. No impurity phases were found in the spectra. The Raman results concurred with the XRD analysis.

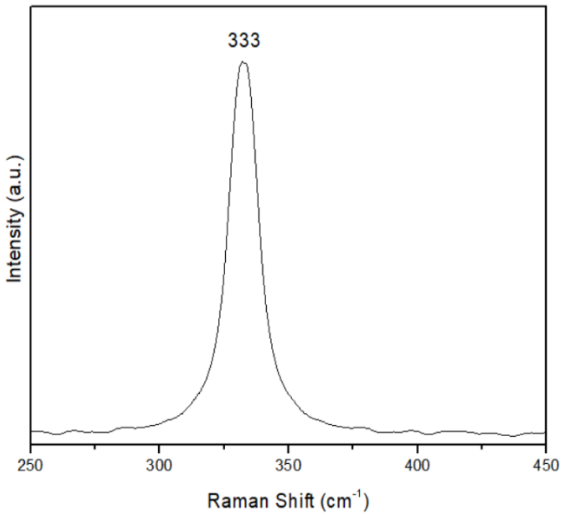

Fig. 2. Raman spectrum of Cu_2MgSnS_4 films deposited with nitrogen.

Fig.3 indicates the SEM micrographs of Cu_2MgSnS_4 thin films prepared with two-carrier gases. The films are found to have a densely packed and almost uniform grain structure. Most importantly, grain morphology improved when nitrogen was employed in the deposition [29]. This kind of improvement resulted in the formation of dense and continuous grain networks, which are found to be favorable for optoelectronic device applications [30].

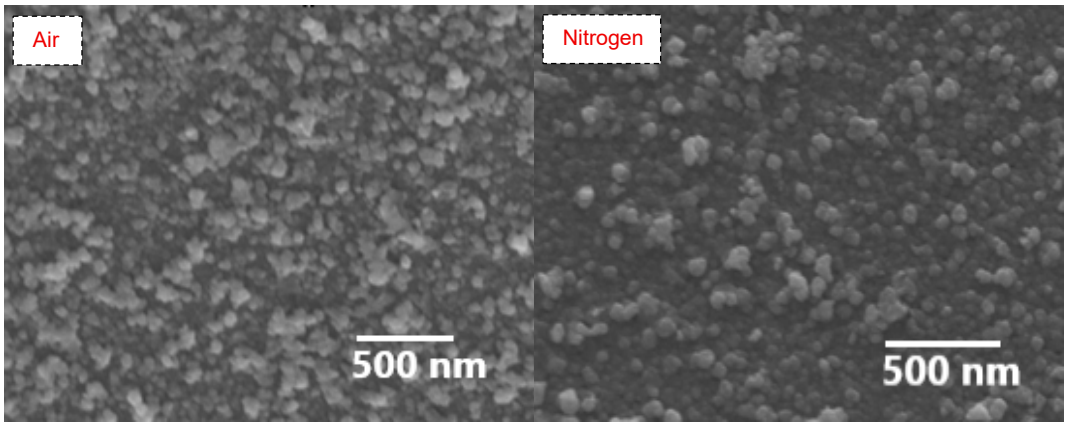

Fig. 3. SEM images of Cu_2MgSnS_4 thin films deposited with air and nitrogen carrier gases.

Fig. 4 (a) and (b) show the transmission and absorption coefficient spectra of Cu_2MgSnS_4 thin films deposited using nitrogen. The absorption coefficient (α) and energy band gap were calculated using standard analytical relationships.

$$\alpha = \ln \frac{(1-R)^2}{T} * \frac{1}{t} \tag{6}$$

where R refers to reflectance, T refers to transmittance, and t is thickness [12,31].

$$(\alpha h\nu) = A(h\nu - Eg)^{\frac{1}{2}} \tag{7}$$

High optical absorption was observed in the films, whose magnitude was higher than 10^5 cm^{-1}. The linear part of the Tauc plot was used to extrapolate and find the direct band gap of the material [32]. Fig. 5 illustrates a comparison of the energy gap of Cu_2MgSnS_4 films synthesized at two carrier gases. The films that were deposited by air demonstrated an energy gap of 1.60 eV, while those deposited under nitrogen had a slightly lower band gap of 1.55 eV. These results are concurred with other reported optical band gap values [8,12], which confirm the suitability of Cu_2MgSnS_4 for photovoltaic applications.

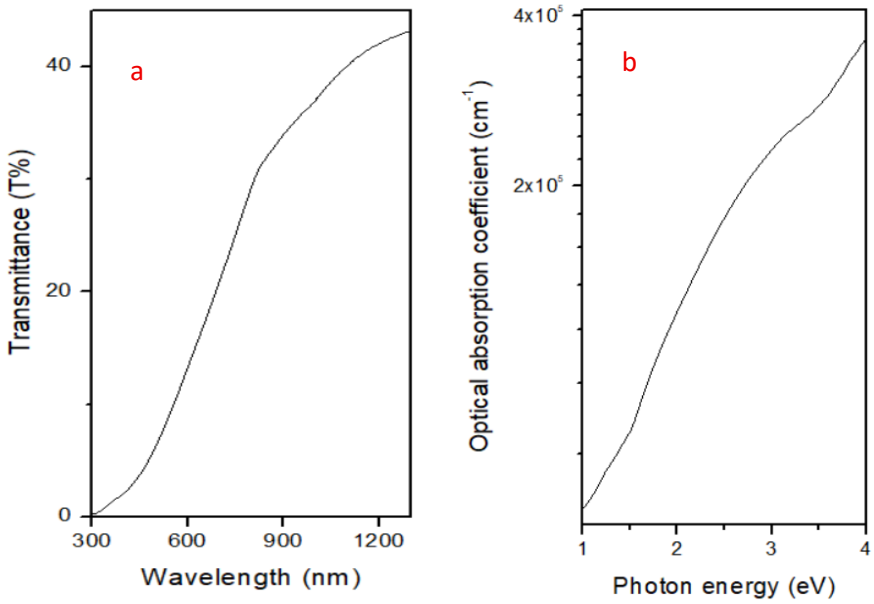

Fig. 4. Transmission spectra and absorption coefficient spectra of Cu_2MgSnS_4 thin films grown using nitrogen.

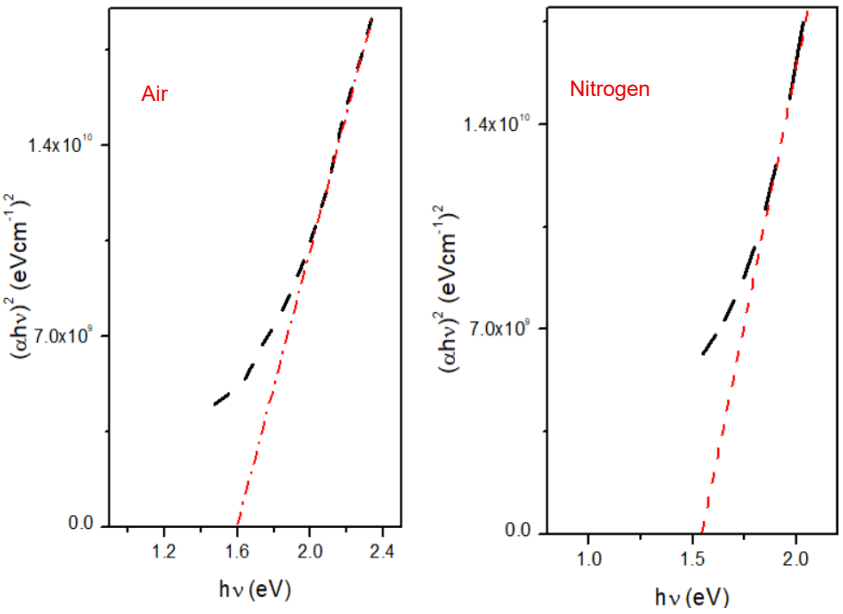

Fig. 5. Energy gap of Cu_2MgSnS_4 thin films synthesized with two carrier gases.

Cu_2MgSnS_4 solar cell was fabricated with a layered structure consisting of glass/MO/CMTS/ CdS/Ag. The absorber layer consisted of the CMTS films deposited using nitrogen. CdS thin film acting as the buffer layer was prepared by the CBD technique [31]. The solar cell demonstrated an open-circuit voltage of 156 millivolts and a short-circuit current density of 1.22 milliamperes per square centimeter. The obtained parameters were suboptimal, indicating the need for further optimization across various studies to improve the quality of the cell parameters.

4. Conclusion

Cu_2MgSnS_4 films were successfully prepared via spray pyrolysis using air and nitrogen as carrier gases, with notable differences in structural and compositional characteristics. Nitrogen as a carrier gas resulted in films with significantly reduced copper content and higher sulfur, helping suppress secondary phases and improving film stoichiometry. XRD analysis confirmed enhanced crystallinity and structural ordering under nitrogen, supported by larger crystallite size, reduced microstrain, and lower dislocation density. Raman spectra showed a strong peak at 333 cm^{-1}, confirming phase purity. SEM images revealed improved grain morphology and compact film structure under nitrogen conditions. Optical analysis demonstrated high absorption coefficients ($>10^5$ cm^{-1}) with a slightly reduced band gap (1.55 eV) for nitrogen-grown films, ideal for solar applications. The solar cells incorporating nitrogen-based CMTS films showed promising photovoltaic potential.

References

[1] Y. B. K. Kumar, D. Nagamalleswari, G. S. Babu, Physica B: Condensed Matter, **645**, 414263 (2022); https://doi.org/10.1016/j.physb.2022.414263
[2] Y. Jayasree, K. Yb Kishore, G. Babu, P. Bhaskar, Physica B: Condensed Matter, **618**, 413199 (2021); https://doi.org/10.1016/j.physb.2021.413199
[3] D. Nagamalleswari, Y. B. K. Kishore, Y. B. Kiran, B. G. Suresh, Chalcogenide Letter **17**(10), 505 (2020).
[4] A. A. Rafal, N. A. Bakra, D. D. Kiran, Chalcogenide Letters **19**(10), 691 (2022); https://doi.org/10.15251/CL.2022.1910.691
[5] Y. Romanyuk, S. Haass, S. Giraldo, M. Placidi, D. Tiwari, D. Fermin, X. Hao, H. Xin, T. Schnabel, M. Kauk-Kuusik, P. Pistor, S. Lie, L. Wong, J. Phys.: Energy **1,** 044004 (2019); https://doi.org/10.1088/2515-7655/ab23bc
[6] M. Souli, R. Engazou, L. Ajili, N. K. Turki, Superlattices and Microstructures, **147**, 106711 (2020); https://doi.org/10.1016/j.spmi.2020.106711
[7] D. Sarra, E. Aubry, N. Bitri, F. Chaabouni, P. Briois, Coatings **10**, 963 (2020); https://doi:10.3390/coatings10100963
[8] A. Hammoud, A. Jrad, B. Yahmadi, M. Souli, F. Kouki, L. Ajili, N. Turki, Optical Materials, **127**, 112296 (2022); https://doi.org/10.1016/j.optmat.2022.112296
[9] A. Hammoud, B. Yahmadi, M. Souli, S. Ahmed, L. Ajili, N. Turki, Eur. Phys. J. Plus **137**, 232 (2022); https://doi.org/10.1140/epjp/s13360-022-02417-z
[10] N. Aravind, R. Roy, K. Kathir, E. Jose, M. C. S. Kumar, Semiconductor Science and Technology, **39**(12), 125017 (2024); https://doi.org/10.1088/1361-6641/ad9173
[11] Y. Gang, X. Zhai, Y. Li, B. Yao, Z. Ding, R. Deng, H. Zhao, L. Zhang, Z. Zhang, Materials Letters **242**, 58 (2019); https://doi.org/10.1016/j.matlet.2019.01.102
[12] A. Ziti, B. Hartiti, A. Belafhaili, H. Labrim, S. Fadili, A. Ridah, M. Tahri, P. Thevenin, Applied Physics A **127**:663 (2021); https://doi.org/10.1007/s00339-021-04824-y
[13] A. Sharma, P. Sahoo, A. Singha, S. Padhan, G. Udayabhanu, R. Thangavel, Solar Energy **203**, 284 (2020); https://doi.org/10.1016/j.solener.2020.04.027
[14] G. Yixin, W. Cheng, J. Jiang, S. Zuo, F. Shi, J. Chu, Materials Letters **172**, 68 (2016); http://dx.doi.org/10.1016/j.matlet.2016.02.088

[15] W. Ming, Q. Du, R. Wang, G. Jiang, W. Liu, C. Zhu, Chem. Lett. **43**, 1149 (2014); http://dx.doi.org/10.1246/cl.140208
[16] A. Ahsan, Y. Liang, S. Ahmed, B. Yang, B. Guo, Y. Yang, Applied Materials Today **18**, 100534 (2020); https://doi.org/10.1016/j.apmt.2019.100534
[17] H. Guan, J. X. Xu, Z. Y. Yang, X. Y. Qian, M. Q. Zhao, Chalcogenide Letters **21**(2), 169 (2024); https://doi.org/10.15251/CL.2024.212.169
[18] V. M. Reddy, P. M. Reddy, G. P. Reddy, G. Sreedevi, K. K. YBReddy, P. Babu, W. K. Kim, K. T. R. Reddy, C. Park, J. Ind. Eng. Chem. **76**, 39 (2019); https://doi.org/10.1016/j.jiec.2019.03.035
[19] D. Nagamalleswari, K. Yb Kishore, Y. B. Kiran, S. Babu, Energy Sources, Part: A Recovery, Util. Environ. Eff. **41**, 3001 (2019); https://doi.org/10.1080/15567036.2019.1583294
[20] U. Chalapathi, S. Sambasivam, Y. B. K. Kumar, R. Cheruku, P. Kondaiah, M. Lavanya, V. Gonuguntla, S. Alhammadi, M. Albaqami, M. Sheikh, S. Park, Optical Materials **152**, 115492 (2024); https://doi.org/10.1016/j.optmat.2024.115492
[21] H. Katagiri, K. Saitoh, T. Washio, H. Shinohara, T. Kurumadani, S. Miyajima, Sol. Energy Mater. Sol. Cells **65**, 141 (2001); https://doi.org/10.1016/S0927-0248(00)00088-X
[22] D. Nagamalleswari, Y. Kumar yb, V. Ganesh, Physica B **616**, 413119 (2021); https://doi.org/10.1016/j.physb.2021.413119
[23] S. G. Prasad, A. S. S. Smitha, U. Chalapathi, G. S. Babu, Y. Jayasree, P. U. Bhaskar, Si-Hyun Park, K. Kishore yb, Chalcogenide Letters **21**(9), 719 (2024); https://doi.org/10.15251/CL.2024.219.719
[24] JCPDS file No. 98-017-1983
[25] K. Kishore yb, G. S. Babu, U. Chalapathi, Y. B. Kiran, P. Uday Bhaskar, Si-Hyun Park, Physica B **670,** 415366 (2023); https://doi.org/10.1016/j.physb.2023.415366
[26] H. Ahmoum, P. Chelvanathan, M. S. Su'ait, M. Boughrara, G. Li, A. H. A. Al-Waeli, K. Sopian, M. Kerouad, N. Amin, Superlattice. Microst. **140**, 106452 (2020); https://doi.org/10.1016/j.spmi.2020.106452
[27] M. A. Islam, K. S. Rahman, F. Haque, M. Akhtaruzzaman, M. M. Alam, Z. A. Alothman, K. Sopian, N. Amin, Chalcogenide Lett. **11**, 233 (2014);
[28] H. Gencer, M. Gunes, A. Goktas, Y. Babur, H. I. Mutlu, S. Atalay, J. alloys and compounds **465**,20 (2008); https://doi.org/10.1016/j.jallcom.2007.10.110
[29] N. Katariya, B. Singh, A. Saxena, V. Ganesan, Macromolecular Symposia **407**(1), 2100473 (2023); https://doi.org/10.1002/masy.202100473
[30] V. G. Rajeshmon, M. R. Rajesh Menon, C. Sudhakartha, K. P. Vijayakumar, J. Anal. Appl. Pyrol. **110**, 448 (2014); https://doi.org/10.1016/j.jaap.2014.10.014
[31] V. S. Raja, K. Yb Kishore, Surfaces and Interfaces **9**, 233 (2017); http://dx.doi.org/10.1016/j.surfin.2017.10.003
[32] U. Chalapathi, K. Yb Kishore, S. Uthanna, V. Sundara Raja, AIP Conf. Proc. 1447, 649 (2012); http://dx.doi.org/10.1063/1.4710170